

Spherical albedo of a Lommel-Seeliger scattering ellipsoidal asteroid

Karri Muinonen^{1,2} and Olli Wilkman¹

¹Department of Physics, University of Helsinki,
Gustaf Hällströmin katu 2a, P.O. Box 64, FI-00014 U. Helsinki, Finland
email: karri.muinonen@helsinki.fi

²Finnish Geospatial Research Institute,
Geodeetinrinne 2, FI-02430 Masala, Finland

Abstract. We compute the spherical albedo for a Lommel-Seeliger scattering ellipsoidal asteroid with a realistic disk-integrated phase function. The spherical (or Bond) albedo gives the ratio of the fluxes incident on and scattered by an asteroid. Thus, it plays a key role in the determination of the flux absorbed and afterwards thermally emitted by the asteroid at longer wavelengths. We provide extensive computations for the spherical albedo of low-albedo and moderate-albedo asteroids by utilizing the analytical disk-integrated brightness of a Lommel-Seeliger ellipsoid. In doing so, we utilize realistic triaxial models of known asteroids as well as idealistic prolate or oblate models of substantial elongation or flatness, respectively. We show that the spherical albedos can vary significantly as a function of the rotational pole orientation, rotational phase, and the triaxial ellipsoidal shape: variations of the order of 5-10% are realistic, with a tendency to grow with increasing elongation or flatness of the shape.

Keywords. Minor planets, asteroids, solar system: general, radiative transfer, scattering, methods: analytical, methods: numerical, techniques: photometric

1. Introduction

The ellipsoid captures an asteroid's shape in three dimensions with only two parameters, that is, the axial ratios b/a and c/a , where a , b , and c denote the semiaxes of the ellipsoid. The ellipsoid is thus an appealing overall model for an asteroid's shape, a statement supported by the scientific preparation for the Gaia space mission (Cellino *et al.* 2009, Carbognani *et al.* 2012, Cellino *et al.* 2015, Muinonen & Lumme 2015, Muinonen *et al.* 2015) and earlier work in shape and rotational pole determination (Drummond *et al.* 1988, Magnusson *et al.* 1989).

The disk-integrated brightness of an ellipsoidal asteroid is analytically available for a Lommel-Seeliger surface scattering model, that is, in the case of dark, particulate surfaces typical for, e.g., primitive asteroids (Muinonen & Lumme 2015). The Lommel-Seeliger model follows from the radiative-transfer theory in the case of small single-scattering albedo, allowing us to omit the orders of scattering higher than the first (Chandrasekhar 1960). The analytical disk-integrated brightness has given rise to novel initial methods for asteroid lightcurve inversion (Cellino *et al.* 2015, Muinonen *et al.* 2015) in the case of sparse photometric data.

In Section 2, we review the photometric properties of the triaxial Lommel-Seeliger ellipsoid, including the disk-integrated brightness, geometric albedo, and the spherical albedo (or Bond albedo). In Section 3, we describe extensive computations for the spherical albedo as a function of rotational pole orientation, rotational phase, as well as the ellipsoid axial ratios. Finally, in Section 4, we provide the conclusions of the study.

2. Photometry with a Lommel-Seeliger Ellipsoid

We begin with the reflection coefficient R of a surface element that relates the incident flux density πF_0 and the emergent intensity I :

$$I(\mu, \phi; \mu_0, \phi_0) = \mu_0 R(\mu, \phi; \mu_0, \phi_0) F_0, \quad (2.1)$$

$$\mu_0 = \cos \iota, \quad \mu = \cos \epsilon,$$

where ι and ϵ are the incidence and emergence angles as measured from the outward normal vector, and ϕ_0 and ϕ are the corresponding azimuths. We can measure ϕ so that the backscattering direction (or light-source direction) is with $\phi = 0^\circ$. Thus, with the typical additional assumption of a geometrically isotropic surface, specifying ϕ_0 is unnecessary.

The Lommel-Seeliger reflection coefficient (subscript LS) is (e.g., Lumme and Bowell 1981),

$$R_{\text{LS}}(\mu, \mu_0, \phi) = \frac{1}{4} \tilde{\omega} P(\alpha) \frac{1}{\mu + \mu_0}, \quad (2.2)$$

where $\tilde{\omega}$ and P are the single-scattering albedo and phase function, respectively, and α is the phase angle, the angle between the Sun and the observer as seen from the object. The Lommel-Seeliger reflection coefficient is the first-order multiple-scattering approximation from the radiative-transfer theory (e.g., Chandrasekhar 1960). In scalar radiative transfer omitting polarization effects, the phase function P provides the angular distribution of scattered light in an individual interaction and is normalized so that

$$\int_{(4\pi)} \frac{d\Omega}{4\pi} P(\alpha) = 1. \quad (2.3)$$

The disk-integrated brightness L equals the surface integral

$$L(\alpha) = \int_{A_+} dA \mu I(\mu, \mu_0, \alpha) = \int_{A_+} dA \mu \mu_0 R(\mu, \mu_0, \alpha) F_0, \quad (2.4)$$

where A_+ stands for the part of the surface that is both illuminated by the Sun and visible to the observer. For a nonspherical asteroid, L can depend strongly on the orientation of the asteroid with respect to the scattering plane, where L is measured.

For a spherical asteroid with diameter D , we obtain the disk-integrated brightness

$$L_{\text{LS}}(\alpha) = \frac{1}{32} \pi F_0 D^2 \tilde{\omega} P(\alpha) \Phi_{\text{LS}}(\alpha),$$

$$\Phi_{\text{LS}}(\alpha) = 1 - \sin \frac{1}{2} \alpha \tan \frac{1}{2} \alpha \ln \left(\cot \frac{1}{4} \alpha \right), \quad (2.5)$$

where we have also given the phase function $\Phi_{\text{LS}}(\alpha)$ normalized to unity at $\alpha = 0^\circ$.

For an ellipsoidal asteroid with the semiaxes a , b , and c , and $C = \text{diag}(a^{-2}, b^{-2}, c^{-2})$, the disk-integrated brightness is also available in a closed form. Let \mathbf{e}_\odot and \mathbf{e}_\oplus be the unit vectors in the directions of the Sun and the observer, respectively, as seen in the principal-axes reference frame of the ellipsoid. Following Muinonen & Lumme (2015), for the computation of the disk-integrated brightness, we define three sets of auxiliary quantities. First, the solar phase angle follows from

$$\cos \alpha = \mathbf{e}_\odot \cdot \mathbf{e}_\oplus. \quad (2.6)$$

Second, we define two vector-matrix products S_\odot and S_\oplus as well as an angle α' so that

$$S_\odot = \sqrt{\mathbf{e}_\odot^T C \mathbf{e}_\odot}, \quad S_\oplus = \sqrt{\mathbf{e}_\oplus^T C \mathbf{e}_\oplus},$$

$$\cos \alpha' = \frac{\mathbf{e}_\oplus^T \mathbf{C} \mathbf{e}_\oplus}{S_\odot S_\oplus}, \quad \sin \alpha' = \sqrt{1 - \cos^2 \alpha'}. \quad (2.7)$$

Third, we define an amplitude S and an angle λ' so that

$$S = \sqrt{S_\odot^2 + S_\oplus^2 + 2S_\odot S_\oplus \cos \alpha'},$$

$$\cos \lambda' = \frac{S_\odot + S_\oplus \cos \alpha'}{S}, \quad \sin \lambda' = \frac{S_\oplus \sin \alpha'}{S}. \quad (2.8)$$

The disk-integrated brightness of a Lommel-Seeliger ellipsoid is then given by

$$L(\alpha) = \frac{1}{8} \pi F_0 \tilde{\omega} P(\alpha) abc \frac{S_\odot S_\oplus}{S} \cdot$$

$$\left\{ \cos(\lambda' - \alpha') + \cos \lambda' + \sin \lambda' \sin(\lambda' - \alpha') \ln \left[\cot \frac{1}{2} \lambda' \cot \frac{1}{2} (\alpha' - \lambda') \right] \right\}. \quad (2.9)$$

The geometric albedo p is the disk-integrated brightness at opposition divided by that of a normally illuminated, perfectly Lambertian disk with the same surface area:

$$p = \frac{L(0^\circ)}{\pi abc S_\odot F_0} = \frac{1}{8} \tilde{\omega} P(0^\circ). \quad (2.10)$$

Notice that, for a Lommel-Seeliger ellipsoid, p is constant and independent of the rotational pole orientation, rotational phase, and axial ratios.

Consider next $\tilde{\omega}$ and $P(\alpha)$. Asteroid phase curves suggest that the disk-integrated brightness phase function should be close to the H, G_1, G_2 phase function $\Phi_{HG_1G_2}$ (Muinonen *et al.* 2010). It is now reasonable to assume that the model

$$\frac{1}{8} \tilde{\omega} P(\alpha) = p \frac{\Phi_{HG_1G_2}(\alpha)}{\Phi_{LS}(\alpha)} \quad (2.11)$$

can serve well in asteroid phase-curve analyses (Muinonen *et al.* 2015). Alternatively, as in the present context, we may utilize the H, G_{12} phase function $\Phi_{HG_{12}}$ (Muinonen *et al.* 2010):

$$\frac{1}{8} \tilde{\omega} P(\alpha) = p \frac{\Phi_{HG_{12}}(\alpha)}{\Phi_{LS}(\alpha)}. \quad (2.12)$$

Finally, the spherical albedo A is obtained by integrating the disk-integrated brightness over the full solid angle (corresponding to the integration over the observing directions) and by dividing with the total power incident on the cross-sectional area of the object:

$$A = \frac{1}{\pi F_0 \pi abc S_\odot} \int_{(4\pi)} d\Omega_\oplus L(\alpha) = \int_{(4\pi)} d\Omega_\oplus \frac{1}{8} \tilde{\omega} P(\alpha) \frac{S_\oplus}{S} \cdot$$

$$\left\{ \cos(\lambda' - \alpha') + \cos \lambda' + \sin \lambda' \sin(\lambda' - \alpha') \ln \left[\cot \frac{1}{2} \lambda' \cot \frac{1}{2} (\alpha' - \lambda') \right] \right\}$$

$$= \frac{p}{\pi} \int_{(4\pi)} d\Omega_\oplus \frac{\Phi_{HG_1G_2}(\alpha)}{\Phi_{LS}(\alpha)} \frac{S_\oplus}{S} \cdot$$

$$\left\{ \cos(\lambda' - \alpha') + \cos \lambda' + \sin \lambda' \sin(\lambda' - \alpha') \ln \left[\cot \frac{1}{2} \lambda' \cot \frac{1}{2} (\alpha' - \lambda') \right] \right\}, \quad (2.13)$$

where, when deemed appropriate, the phase function $\Phi_{HG_1G_2}$ can be replaced with the phase function $\Phi_{HG_{12}}$.

| Model | b/a | c/a | A_{\min} | A_{\max} | A_m | δA |
|-------|-------|-------|------------|------------|-------|------------|
| 1C | 0.86 | 0.82 | 1.84 | 1.89 | 1.86 | 2.2 |
| 2C | 0.88 | 0.63 | 1.81 | 1.91 | 1.86 | 5.1 |
| 3C | 1.00 | 0.50 | 1.79 | 1.93 | 1.87 | 7.5 |
| 4C | 0.50 | 0.50 | 1.83 | 1.98 | 1.87 | 8.2 |
| 1S | 0.86 | 0.82 | 8.53 | 8.73 | 8.61 | 2.4 |
| 2S | 0.88 | 0.63 | 8.37 | 8.85 | 8.62 | 5.5 |
| 3S | 1.00 | 0.50 | 8.24 | 8.94 | 8.64 | 8.1 |
| 4S | 0.50 | 0.50 | 8.44 | 9.20 | 8.63 | 8.9 |

Table 1. The ellipsoid axial ratios b/a and c/a and the minimum, maximum, and mean spherical albedos A_{\min} , A_{\max} , and A_m (all in %) of the ellipsoid, respectively, as well as the relative variation δA (%), for four different shapes (1–4) and the two different spectral types (C and S). See text.

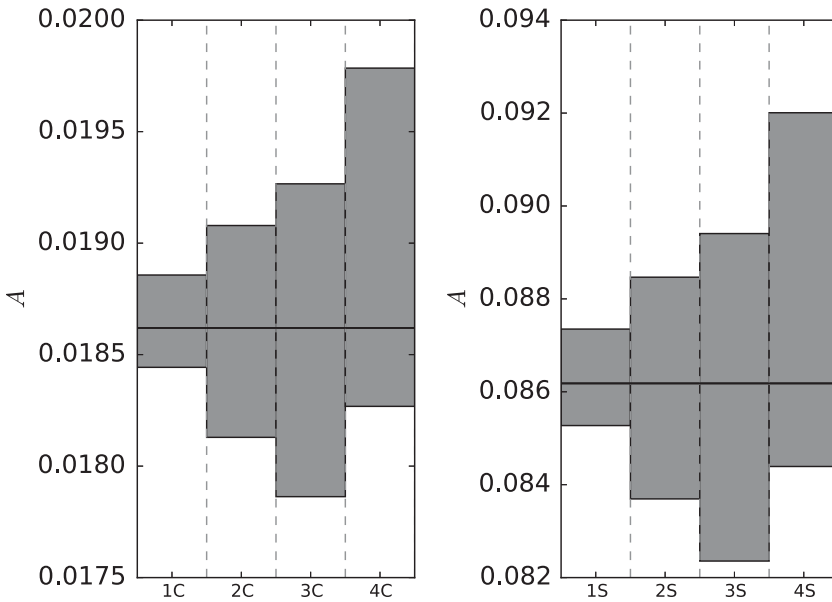


Figure 2. The range of A for the different models. Grey bars show the range between the minimum and maximum values around the values for the spherical models (black lines).

Figure 2 and Table 1 show the range of variation of A for each model. These values represent the maximum variation over all values computed over every pole orientation and rotational aspect. A is seen to vary around the value for spheres. The relative variation of the spherical albedo,

$$\delta A = \frac{A_{\max} - A_{\min}}{A_S}, \tag{3.1}$$

depends mostly on the shape. For a given shape, δA does not change much between the C- and S-types. The maximum variations of spherical albedo for a single object are almost 9%. Averaging the spherical albedo over one rotation does not change the numbers of Table 1 within the precision they are given.

4. Conclusion

We have computed the spherical albedo for ellipsoidal asteroids that scatter light according to the Lommel-Seeliger first-order multiple-scattering model with a realistic phase function. The results show that variations in the spherical albedo of the order of 10% can be expected.

In the future, we plan to compute reference spherical albedos for ellipsoidal asteroids as averages over all orientations weighted by the cross-sectional area of each orientation. We aim toward extending the present analysis further by incorporating the numerical particulate-medium scattering model by Wilkman *et al.* (2015), where the surface porosity and roughness are accounted for in detail. Extensive computations of spherical albedo are made possible by the rapid utilization of the scattering models via interpolation in a pre-computed grid of porosity and roughness parameter values.

Acknowledgements

Research supported, in part, by the Academy of Finland (grant No. 1257966).

References

- Carbognani, A., Tanga, P., Cellino, A., Delbó, M., Mottola, S., & Marchese, E. 2012, *Planet. Space Sci.* 73, 80, doi:10.1016/j.pss.2011.12.002
- Cellino, A., Hestroffer, D., Tanga, P., Mottola, S., & Dell'Oro, A. 2009, *Astron. Astrophys.* 506, 935, doi:10.1051/0004-6361/200912134
- Cellino, A., Muinonen, K., Hestroffer, D., & Carbognani, A. 2015, *Planet. Space Sci.*, 118, 221, doi:10.1016/j.pss.2015.09.004
- Chandrasekhar, S., 1960, *Radiative Transfer* (Dover, New York)
- Drummond, J. D., Weidenshilling, S. J., Chapman, C. R., & Davis, D. R. 1988, *Icarus* 76, 19, doi:10.1016/0019-1035(88)90139-X
- Lumme, K. & Bowell, E. 1981, *Astron. J.* 86, 1694, doi:10.1086/113054
- Magnusson, P., Barucci, M. A., Drummond, J. D., Lumme, K., Ostro, S. J., Surdej, J., Taylor, R. C., & Zappalà, V. 1989, in: R.P. Binzel, T. Gehrels, & M. S. Matthews (eds.), *Asteroids II* (Univ. of Arizona Press., Tucson), p. 66
- Muinonen, K., Belskaya, I. N., Cellino, A., Delbò, M., Lvasseur-Regourd, A.-C., Penttilä, A., & Tedesco, E. F. 2010, *Icarus* 209, 542, doi:10.1016/j.icarus.2010.04.003
- Muinonen, K. & Lumme, K. 2015, *Astron. Astrophys.*, A23, doi:10.1051/0004-6361/201526456
- Muinonen, K., Wilkman, O., Cellino, A., Wang, X., & Wang, Y. 2015, *Planet. Space Sci.*, 118, 227, doi:10.1016/j.pss.2015.09.005
- Penttilä, A., Muinonen, K., Shevchenko, V. G., & Wilkman, O. 2016, *Planet. Space Sci.*, in press, doi:10.1016/j.pss.2015.08.010
- Shevchenko, V. G., Belskaya, I. N., Muinonen, K., Penttilä, A., Krugly, Y. N., Velichko, F. P., Chiorny, V. G., Slyusarev, I. C., Gaftonyuk, N. M., & Tereschenko, I. A. 2016, *Planet. Space Sci.*, in press
- Torppa, J., Hentunen, V.-P., Pääkkönen, P., Kehusmaa, P., & Muinonen, K. 2008, *Icarus* 198, 91, doi:10.1016/j.icarus.2008.07.014
- Wilkman, O., Muinonen, K., & Peltoniemi, J. I. 2015, *Planet. Space Sci.*, 118, 250, doi:10.1016/j.pss.2015.06.004